Unusual Confinement-Induced Basicity and Proton-Mediated CH Activity of an Adipic Acid-Ammonium Cluster

John J. Kreinbihl,[†] Nicoline C. Frederiks,[†] Kathleen A. Nickson,[†] Annapoorani Hariharan,[†] Emily E. Racow,[†] Melanie Chiu,[†,‡] and Christopher J. Johnson[*,†]

†*Department of Chemistry, Stony Brook University, Stony Brook, NY 11790*

‡*Current address: Department of Chemistry, Michigan State University, East Lansing, MI 48824*

E-mail: chris.johnson@stonybrook.edu

Abstract

Organic acids play an important role in atmospheric chemistry, particularly in the formation of aerosol particles. They are often detected with hydronium, ammonium, or nitrate chemical ionization sources, which are generally soft ionization sources but may cause fragmentation. Here we explore the reactivity of adipic acid, an analogue to the α-pinene oxidation product pinic acid, upon complexation with ammonium. Mass spectra and mass-selective vibrational spectra show that even mild activation, consistent with normal operation of an electrospray ionization source, yields (adipic acid)H^+ and neutral ammonia. This is traced to a specific structural motif in which both protonated carboxylic acid carbonyl groups combine to form a site that is locally more basic than ammonia. Further mild collisional activation yields sequential loss of two water molecules, the known behavior of carboxylic acids in superacids, necessitating abstraction of at least one hydrogen from a CH group. Deuterium labeling experiments

confirm that the second step indeed involves CH hydrogen atoms. Comparison of vibrational spectra and quantum chemical calculations allows us to assign structures for each step, identifying several ring structures but notably not forming the minimum energy structure upon the first loss of water. ESI of a range of linear dicarboxylic acids shows this to be a common feature of this class of organic acids. We propose a mechanism that explains this reactivity and discuss possible atmospheric implications of these observations.

Introduction

Atmospheric aerosols have have a pronounced effect on both human health and Earth's climate.[1,2] Aerosol effects currently represent the largest source of error in climate change models.[3]

Organic compounds may accelerate growth in particle processes, but the mechanism by which they are involved is not well understood.[4–9] Secondary organic aerosols (SOA), aerosols formed by volatile organic compounds (VOCs) undergoing gas-to-particle transfer, constitute a significant portion of all tropospheric aerosols.[10–12] The primary complication stems from the role of VOCs which are thought to photooxidize or chemically oxidize in the atmosphere to yield lower volatility products that then form SOA. Estimates suggest that between 10,000 and 100,000 different organic compounds are found in the atmosphere, and each VOC can undergo a number of different degradation pathways yielding different oxidation products, which greatly complicates their inclusion in any modeling attempts.[9,12] Recently, it has been established that extremely-low volatility organic compounds (ELVOCs), believed to be formed through consecutive internal hydrogen shift reactions that facilitate autoxidation reactions, play a critical role in organic enhanced nucleation.[13–15]

The majority of studies on the impact of VOCs in the atmosphere are focused on terpenes, in particular α-pinene, which is emitted from pine forests.[9,12] A particular ozonolysis product of α-pinene, pinic acid, has become a prototypical NPF-relevant organic acid.[16,17]

Computational results have suggested that clusters of pinic acid and sulfuric acid are highly stabilized by hydrogen bonds, and estimates of the Gibbs free energies of formation suggest that pinic acid's primary role is in the growth of clusters rather than the nucleation of new clusters.[9] However, there are few experimental benchmarks with which to compare these results.

A photoelectron spectroscopy study probed the microsolvation of cis-pinate, another photooxidation product of α-pinene, with various solvents and demonstrated a careful balance between solute-solvent and solvent-solvent interactions unique to the gas-phase.[18] This suggests that the environment plays a key role in the structures and pathways of the clusters in the atmosphere and is unlike those found in the bulk. Other work has begun to explore the itermolecular interactions of organic acids in small clusters.[19–21]

Chemical ionization (CI) sources are common mechanisms to ionize free vapors and small particles, and are considered to be "soft" ionization sources that impart little energy into the analyte. Typically employing protonated ammonia or water clusters for analytes with basic sites and nitrate for analytes with acidic sites, ion-molecule proton transfer reactions drive the ionization process. While soft, this process may still be energetic enough to drive dissociative chemistry, and the atmospheric pressure interface of common commercial instruments have been shown to be mildly activating,[22] suggesting that CI mass spectra may not fully represent the gas phase species being sampled.[23]

Diprotonated carboxylic acids have been observed in the presence of superacids[24,25] and in the gas phase.[26,27] These diprotonated species show interesting properties, for instance enhancing the reactivity of adjacent carbocationic sites and exhibit superelectrophilic reactivity.[28,29] Rearrangement of the protonated carboxylic acid to produce H_2O and an acylium ion is observed in both the condensed and gas phases.[24,30]

In this work, we employ collision-induced dissociation (CID) mass spectrometry to probe the behavior of adipic acid, an inexpensive analogue to pinic acid.[31] We isolate protonated adipic acid and an adipic acid-ammonia compound in a ion trap and perform up to MS^4

experiments to determine the decomposition products of the cluster. We then use cryogenic ion vibrational predissociation (CIVP) spectroscopy and density functional theory (DFT) calculations to determine the structure of each product, leading to a proposed mechanism describing the decomposition pathway.

Experimental Section

Ammonium-adipic acid clusters were prepared using solutions of the following reagents: >99.0% adipic acid from Merck Millipore, HPLC grade water from Fisher Scientific, 99.9% deuterium oxide (D_2O) from Sigma Aldrich, HPLC grade 99.8% acetonitrile, LC/MS formic acid in H_2O from Fisher Scientific, and 95 wt. % formic acid from Sigma Aldrich.

All collision-induced dissociation (CID) experiments were conducted using a Thermo Scientific LTQ XL ion trap mass spectrometer. Adipic acid clusters were generated by electrospray ionization (ESI) of a solution of 5 mM solution of adipic acid in water with 0.1 wt.% formic acid. Ammonia was presumably sourced from the atmosphere or trace contaminants in the solute or solvent. For CID experiments, the ammonium-adipic acid cluster was isolated and activated with enough Normalized Collision Energy (NCE, a non-standard unit that provides a relative energy scale) to dissociate approximately 90% of the parent ion. For MS^n experiments, this process was repeated for the specified number of CID cycles. Clusters containing deuterium were generated by ESI of a 5 mM adipic acid in deuterium oxide with 0.1% formic acid solution.

Cryogenic ion vibrational predissociation (CIVP) spectra were collected using a home built photofragmentation mass spectrometer described previously.[32,33] Ammonium-adipic acid clusters were generated by ESI of a 2.5 mM solution of adipic acid in 20:80 water:acetonitrile with 0.1% formic acid. These ions were then introduced into the vacuum system and accumulated in a room temperature octopole trap. The RF amplitude and bias of this trap can be tuned to either promote or suppress CID. Ions are then routed from this

trap to a variable-temperature octopole ion trap capable of achieving temperatures between 3 - 310 K. Messenger tagging with N_2 was achieved by storing the clusters of interest in the ion trap held between 20 - 50 K under a pulsed helium buffer gas. Here N_2 is likely sourced from background gas in the vacuum chamber (base pressure 10^{-8} torr). The tagged ions are extracted from the ion trap and orthogonally accelerated into a tandem time-of-flight mass spectrometer consisting of both a linear and reflectron stage. As the ions of interest cross the time focus of the linear stage, they are intersected by an infrared laser pulse from an Nd:YAG pumped infrared OPO/OPA (LaserVision) laser system. The reflectron stage separates fragments from undetached parent ions, which are then guided into a microchannel plate detector. Spectra are obtained by dividing the integrated intensity of the fragment by the sum of the integrated intensities of both the parent and the fragment. A laser power correction is then applied.

All quantum chemistry calculations were carried out at the CAM-B3LYP/aug-cc-pVDZ level of theory using the Gaussian 16 suite of programs.[34] This level of theory has been shown previously to produce computed vibrational spectra with good agreement to experimental data while maintaining computational efficiency that allows for higher throughput to probe structures of up to 7 components in reasonable time.[35] Computed spectra as presented were convolved with 5 cm^{-1} Gaussian functions to reproduce experimental bandwidths and are not scaled.

Results and Discussion

Protonated clusters of ammonia and adipic acid were initially generated using the LTQ system. It was quickly noted that protonated adipic acid and its water-loss product are readily generated as well, as shown in Figure 1. Isolation of the protonated ammonia-adipic acid cluster yielded a substantial fraction of protonated adipic acid, and CID of the cluster produced a 1:1 yield of protonated adipic acid.

Under ordinary solution-phase conditions, the pKa to add an additional proton to fully protonated adipic acid is expected to be significantly lower than the pKa of ammonia. The generated protonated adipic acid suggests that, in the cluster configuration, adipic acid serves as a better base than ammonia. We hypothesized that this is due to a confinement effect affecting the relative acidity of the protonated site. Similar deprotonated dicarboxylic acid anions have been shown to form ring structures featuring a shared proton linking the two carboxylate moities, and we proposed a similar structure in which an ammonium or proton is shared between the carbonyls of the two protonated carboxylic acid groups.

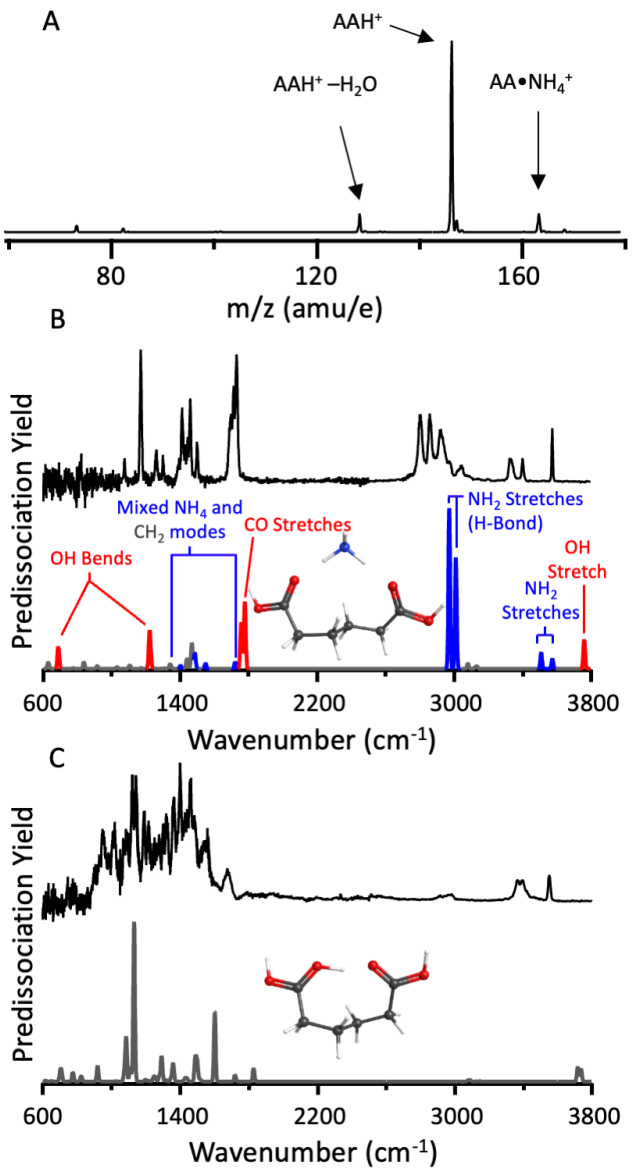

Figure 1: A) The mass spectrum obtained under normal ESI conditions, showing an NH_3 adduct and an H_2O loss product. B) The infrared CIVP spectrum of the N_2-tagged AA(NH_4^+) alongside the calculated harmonic vibrational spectrum of the proposed structure (shown inset). Modes related to the ammonium group are labeled and colored in blue, while modes related to oxygen groups of the adipic acid are labeled and colored in red. C) The infrared CIVP spectrum of the N_2-tagged AAH^+ alongside the calculated harmonic vibrational spectrum of the proposed structure (shown inset).

To probe the structural motifs leading to this unintuitive behavior, CIVP spectra were recorded of both the putative ammonium-adipic acid cluster, shown in Figure 1B, and protonated adipic acid, shown in Figure 1C. Included are the lowest energy structures found through quantum chemical calculations and the corresponding computed harmonic vibrational spectra. Focusing on the ammonium-bound cluster, we find a single sharp feature near 3600 cm^{-1} that is typical for a free OH stretch. At about 3400

cm^{-1} we see a doublet feature that is typical of free NH_2 symmetric and antisymmetric stretches. Between 2500 - 3200 cm^{-1} we see relatively broad features that previous work has assigned to NH_2 stretches for NH_2 groups that are participating in a hydrogen bond.[36] These observations are consistent with the hypothesis of a bridging ammonium. The spectra between 600 - 2500 cm^{-1} are more complex, and here we turn to quantum chemical predictions to assign the rest of the features and confirm the hypothesized structure. Between 600 - 1400 cm^{-1} we see features consisting primarily of OH bending character. Between 1400 - 1700 cm^{-1} the spectral features are typically mixtures of NH_4 and CH_2 bending modes. Around 1800 cm^{-1} we see an intense feature that is likely reflective of CO stretches in the structure. The computed spectrum reproduces well all of the observed features except the hydrogen-bonded NH stretches, which are typically not well represented by harmonic potentials and thus require more sophisticated treatments to accurately reproduce.[37–39]

Turning to the protonated complex, we find that the spectrum is notably harder to parse by inspection. The free OH feature is preserved, but a new feature near 3400 cm^{-1} appears, and the fingerprint region is dominated by a complex feature spanning 700 - 1600 cm^{-1}. This type of feature is common to systems in which a shared proton contributes intensity to a variety of mixed modes, while the energy of the center of this broad feature is indicative of the degree to which the proton is shared between the two oxygen atoms.[40] We attribute the 3400 cm^{-1} feature to tag-induced red shifting of the OH stretch, as the degree of the shift is comparable to previously observed N_2-bound OH stretches.[35,41–43] The broad, lower energy feature is qualitatively consistent with the computed spectrum at the bottom of Figure 1C, though the harmonic spectrum predictably does not reproduce the complexity of the experimental spectrum (Figure S1). We ascribe this feature to a series of anharmonic bands sharing intensity with a strongly-shared proton stretch centered around 1200 cm^{-1}. Such spectral congestion is commonly observed when a strongly absorbing transition is red shifted into resonance with nominally spectroscopically-dark transitions to which it is strongly coupled.[44,45] The spectrum and degree of shift is consistent with observed

shared protons between two *deprotonated* carboxylic acids in dodecanedioic acid.[46]

Taken together, these spectra confirm the possibility that the fully protonated acid can still behave as a base, particularly when confined in a geometry that exposes a binding site bridging the two carboxylic acid carbonyls. This observation adds to the growing library of unintuitive acid base interactions for confined systems confirmed spectroscopically.[47–49]

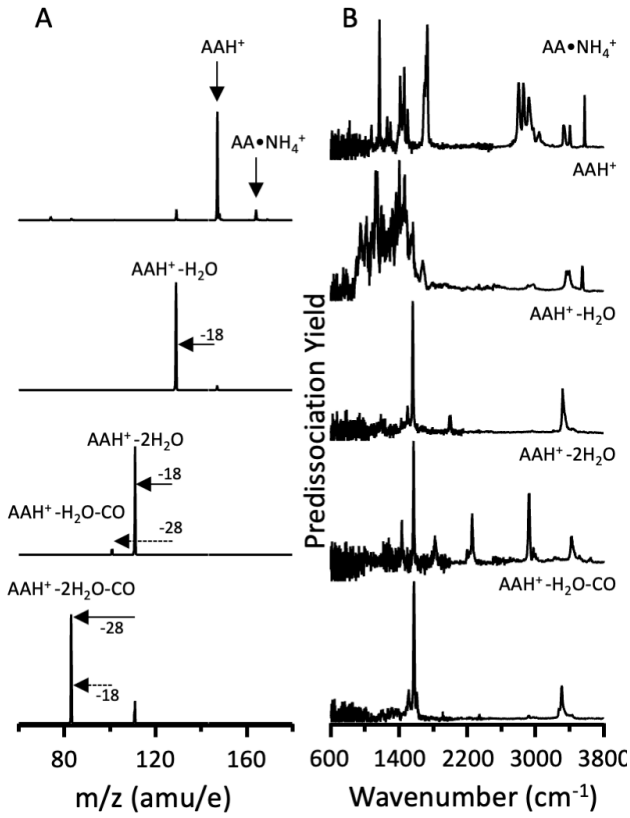

Figure 2: A) The left-hand side of the figure shows a series of mass spectra that, from top to bottom, represent sequential collision-induced dissociation experiments beginning with ammoniated adipic acid, and following through several water loss and CO loss channels. B) The right-hand side of the figure shows the N_2-tagged infrared CIVP spectra of the clusters.

We found that marginally increasing the "harshness" of the ion source by increasing the pressure in the first vacuum region and creating larger potential differences between adjacent electrodes led to the production of additional fragments in conditions that we would not expect fragmentation for typical ESI-sourced molecular ions. We investigated the formation of these fragments using a series of CID experiments. $AA(NH_4^+)$ or AAH^+ was isolated in the LTQ ion trap and fragmented. The same results were found regardless of the species initially isolated, but most experiments discussed here isolated the protonated species initially due to its higher abundance. The primary fragment was then isolated, and fragmented in the same manner until a fragment was created that required significantly higher NCE to dissociate. The resulting mass spectra are shown in Figure 2A. We found dissociation to occur at relatively low NCE more typical of breaking hydrogen bonds (a setting of 10-20 in our instrument). Dissociation proceeds primarily by sequential loss of two water molecules. This observation is unexpected,

as there are only three hydrogen atoms bound to oxygen. Therefore, at least one of the water fragments must contain a hydrogen that originated on the CH backbone. Fragmentation of the second water-loss product leads primarily to loss of CO, terminating the dissociation mechanism for low-NCE excitation. A minor pathway is observed consisting of loss of CO after the loss of only one water, and the fragment produced by CO loss subsequently loses water. Thus, both pathways ultimately converge after the loss of two water molecules and one CO group.

To determine which fragmentation step involves hydrogen originating from a CH_2 group, the same series of CID experiments was conducted on triply-deuterated protonated adipic acid molecules in which the labile oxygen-bound hydrogens were exchanged with deteurium as presented in Figure S2. The first step observed is the loss of D_2O, while the second water lost is found to be either HOD or H_2O indicating that one or two deuterium atoms can remain on the backbone and multiple CH hydrogen-deuterium exchanges may occur.

We generated each of these fragments in our homebuilt photofragmentation mass spectrometer by increasing the pressure and the extraction voltage of the room temperature accumulation octopole. Each fragment was isolated using a quadrupole mass filter, and the CIVP spectra of each was recorded,

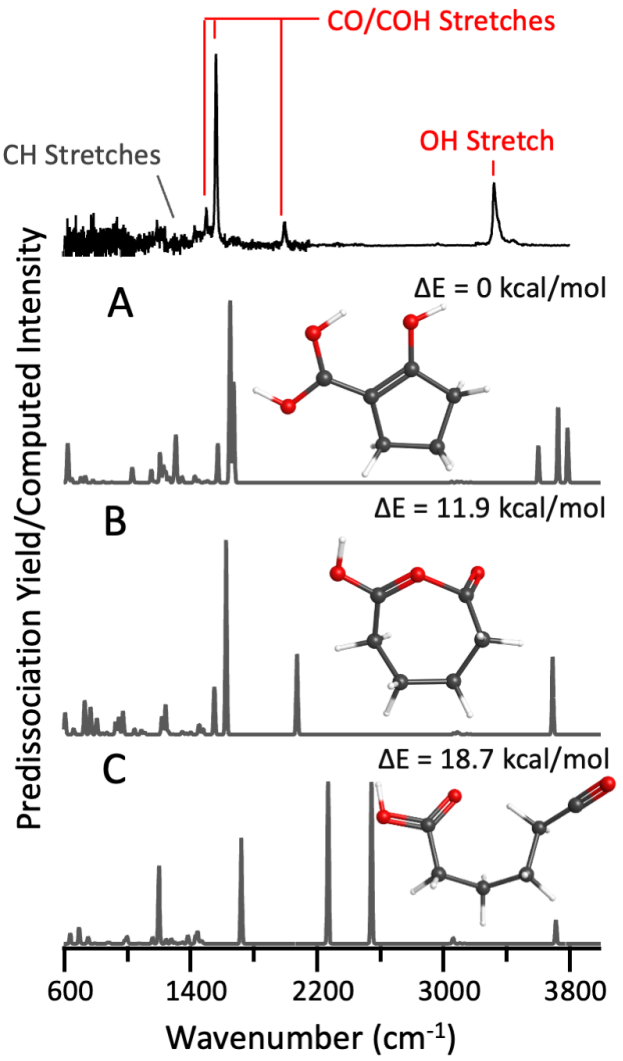

Figure 3: A comparison of the CIVP spectrum of N_2-tagged $AAH^+-(H_2O)$ to the calculated harmonic spectra for three proposed structural arrangements.

as shown in Figure 2B. While the spectra of $AA(NH_4^+)$ and AAH^+ are largely similar, suggesting similar overall structure, the three fragments show substantial spectral changes, suggest significant structural rearrangements occur during the dissociation process.

We expect that several regions of the spectrum should be indicative of the structural motifs in each cluster. For instance, the region of 3550 - 3700 cm^{-1} is highly diagnostic for free OH groups. The region between 1500 - 2500 cm^{-1} typically includes CO stretches that are expected to be sensitive to the precise molecular structure of each cluster.

The CIVP spectrum of $AAH^+{-}H_2O$ is shown in Figure 3 with three potential low-energy structures and their associated computed harmonic vibrational spectra. The spectrum presents as a relatively simple trio of intense features, one in the OH stretching region and two in the fingerprint region. The spectrum is not consistent with the predicted lowest energy structure (A), which features three strong OH stretches and is lacking the feature near 2100 cm^{-1}. This suggests that, on the 100 ms timescale of the experiment, $AAH^+{-}H_2O$ is kinetically trapped. We present two other potential structures that, while higher in energy, both represent unique conformations with improved agreement between experimental and predicted vibrational spectra. The open structure (C) is both higher in energy than the closed structure, and predicts intense shared proton transitions around 2330 and 2660 cm^{-1} that are not observed experimentally. Overall,

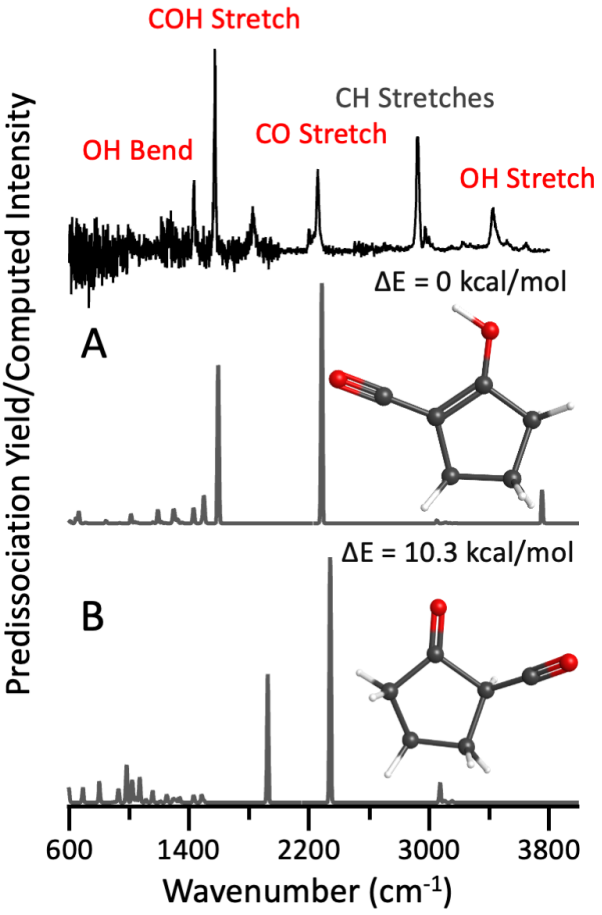

Figure 4: A comparison of the CIVP spectrum of N_2-tagged $AAH^+{-}2\,H_2O$ to the calculated harmonic spectra for two proposed structural arrangements.

the seven-membered ring (B) is the most consistent match to the experimentally observed spectrum. We conclude that structure B is the most likely structure and hypothesize that the minimum-energy structure is not likely to be found due to the presence of a tight transition state for five-membered ring closing, requiring coordinated motions of the hydrocarbon backbone.

The spectrum of $AAH^+ - 2\,H_2O$ is presented in Figure (4) along with the two lowest energy computed structures. The spectrum presents four major bands, an OH stretch around 3400 cm^{-1}, a likely CH stretch around 3000 cm^{-1}, a stretch near 2300 cm^{-1} in a range that would most likely correspond to CO motion, and a peak near 1500 cm^{-1} that is not straightforwardly identified. The computed harmonic vibrational spectrum of the lowest energy structure (A) found is in relatively good agreement with three of these peaks, capturing the major OH, CO, and COH stretches. However, it does not capture the intensity of the CH stretch around 3000 cm^{-1}. On the other hand, a second isomer (B) which is higher in energy, does capture the CH and CO stretches well. Given the prominent OH stretch and anomalously intense CH stretching feature, we suggest that we are observing an isomeric mixture of these two structures. Additional isomers similar to A were computed, in which the double bond was permuted around the ring, but none produced qualitatively different spectra and were significantly higher in

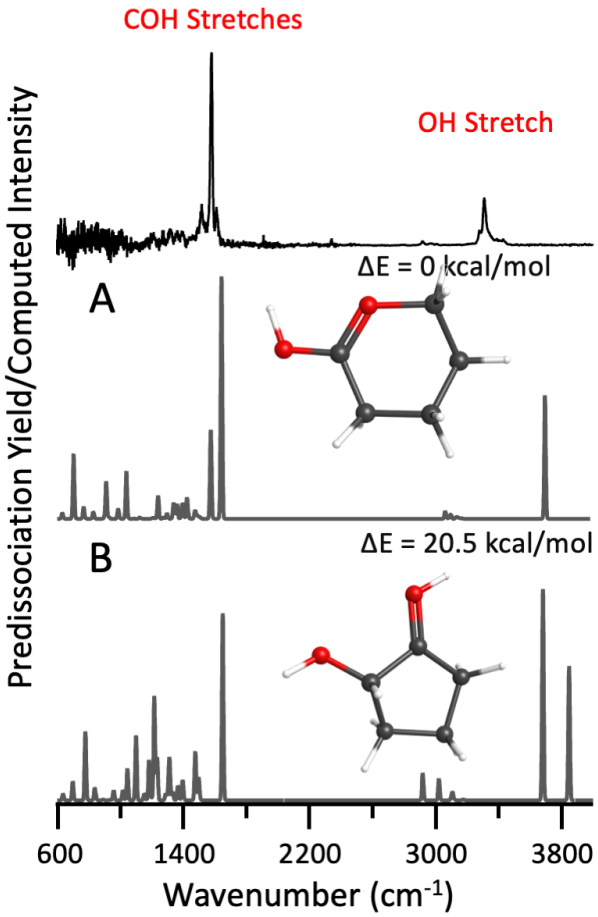

Figure 5: A comparison of the infrared CIVP spectrum of the N_2-tagged, first water-loss and CO-loss fragment from the protonated adipic acid cluster ($AAH^+ - H_2O - CO$) to the calculated harmonic spectra for two proposed structural arrangements.

energy (Figure S3).

The spectrum of AAH^+-H_2O-CO is presented in Figure 5 alongside the two lowest energy computed structures. The experimental spectrum presents two primary features, an OH stretch consistent with that of the fragment of the first water loss, and an intense peak in the region previously ascribed to CO stretching. The computed harmonic vibrational spectrum of the lowest energy structure (A), a six-membered ring, is in good agreement with the observed CIVP spectrum, capturing both the prominent OH stretch and the CO stretches. Recalling that this fragment is produced from the putative seven-membered ring discussed above, rather than the five-membered ring resulting from the second loss of water, this structure seems mechanistically plausible. In fact, the spectra are nearly identical, lacking only the higher energy CO stretching band that is presumably lost as neutral CO upon dissociation. The second lowest energy structure (B) is a five-membered ring significantly higher in energy, and predicts two unique OH stretches that are not observed experimentally. Thus, we assign this spectrum purely to isomer A.

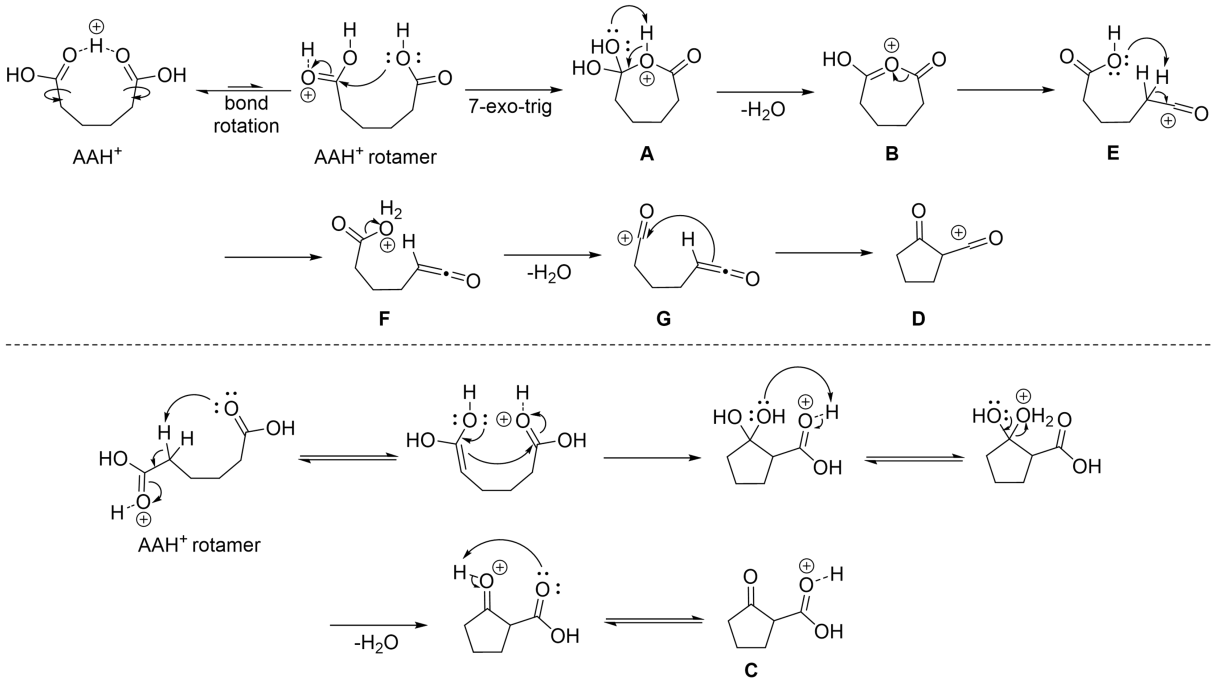

Scheme 1: Top: the proposed mechanism for all CID processes. Bottom: an alternative scheme that would be expected to give rise to the unobserved minimum energy AAH^+-H_2O structure.

One hypothesis for the formation of the observed species is depicted in Scheme 1 and features intramolecular nucleophilic attack of a protonated adipic acid rotamer (AAH^+ rotamer) via 7-exo-trig cyclization, followed by intramolecular dehydration of orthoester **A** to form protonated cyclic anhydride **B**. The initial intramolecular cyclization, which involves attack on an electrophilic carbonyl group, may be kinetically favored over a potential, competing intramolecular deprotonation and aldol-like reaction that would yield the unobserved, but thermodynamically more favored β-ketoacid **C** (Scheme 1, bottom). The observed transformation of protonated cyclic anhydride **B** to the final cyclopentanone product **D** could arise from ring-opening to yield acyl cation **E**. The positive charge on the carbonyl carbon in **E** would increase the acidity of the vicinal proton, enabling intramolecular deprotonation to form ketene **F**.[50] Subsequent dehydration and nucleophilic attack on the resultant acyl cation would afford cyclopentanone **E**. This mechanism is consistent with the experimental isotope scrambling observations, as the initial water loss in triply deuterated adipic acid involves only deuterons on labile oxygens to yield D_2O, but the second water loss involves deprotonation of the carbon backbone, and therefore yields HOD or H_2O.

Finally, we sought to determine if this reactivity was unique to adipic acid or common to dicarboxylic acids. Figure 6 presents the ESI mass spectra of a series of linear dicarboxylic acids containing 1-5 methylene groups (C3-C7, respectively, in Figure 6) under typical conditions without additional activation. We find that each does indeed lose a water molecule, noting a slight trend of increasing yield with increasing chain length. This presumably reflects a reduction of steric hindrance for the longer chains. As we show in the Supplementary Information, these species also undergo similar sequential loss of two

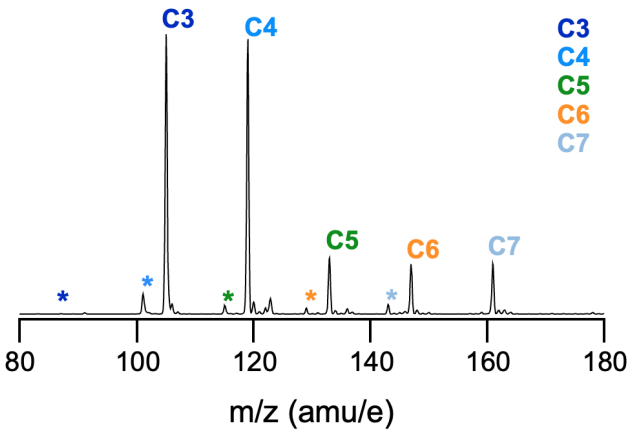

Figure 6: ESI MS of a mixture of linear dicarboxylic acids CN: $H^+HOOC(CH_2)_{N-2}COOH$ (N=3-7). * denotes the yield of H_2O loss under normal ESI operation (no additional activation).

water molecules and loss of CO upon CID, consistent with our observations of protonation adipic acid.

Taking these results into account, we are able to identify several potentially interesting lessons from the dissociation of adipic acid. First, the loss of ammonia creating protonated adipic acid suggests that dramatic changes in basicity can be caused by specific conformational motifs potentially found in atmospherically-relevant clusters as compared to bulk solution or larger particles. It is possible that this confinement-induced basicity effect could be common in both small clusters and, potentially, rough surfaces of small particles. Second, acid-induced reactivity may yield unexpected products in particularly acidic environments. Aerosols have been found to be protonated at levels consistent with pH values near zero,[51,52] and specific sites may be expected to be even more acidic. Third, the proposed ring-closing reaction we observe could simply be an artifact of the unimolecular nature of this obseservation. This implies that dimer-forming reactions may occur in clusters of multiple organic acids or particle surfaces. This would significantly reduce the vapor pressure of acid molecules in those clusters or particles, leading to enhanced stability and growth rates. Finally, we note that the readily-achieved water loss from the cluster also facilitates an aging-related reduction in the O:C ratio of the cluster. Taken together, these observations speak to the complexity of the behavior of acidic clusters in the atmosphere.

Conclusion

In this work, we investigated the evolution of clusters of ammonium and adipic acid under mildly activating thermodynamic conditions that might be present in typical CIMS instruments. In the cluster geometry, we have observed adipic acid serving as a stronger base than ammonia in the gas phase. This is consistent with similar suggestions of pinic acid acting as a base in pinic acid - sulfuric acid clusters[9] and suggests that the specifics of the gas phase can complicate traditional views on relative basicity from solution-based perspectives. This

dramatic change is basicity is likely driven by the conformation of the ammonium-adipic acid complex, and this type of conformational change in basicity could be present in many small clusters or potential particle surfaces.[47,48]

We demonstrate that the breakdown of adipic acid in the presence of an extra proton occurs via a complex set of internal hydrogen shifts, suggesting a possible new route for the formation of ELVOCs in the atmosphere and further supporting the notion that hydrogen shifts are crucial in understanding the role of organic compounds in the atmosphere. This acid-induced reactivity may be present in other particularly acidic clusters or on particle surfaces.

Taken together, these results show that clusters make up a laboratory for accessing potentially unique organic chemistry that involves unusual acid-base interactions and confinement effects that may have significant atmospheric ramifications justifying further investigation.

Supplementary Material

Figures comparing anharmonic and harmonic calculations to the experimental spectrum of $AAH^+ - H_2O$, results of CID experiments on AAH^+-d_3, comparing computed spectra for different double bond locations in $AAH^+ - 2\,H_2O$, CID spectra for C3-C7 dicarboxylic acids, and coordinates for all computed structures.

Acknowledgements

J.J.K., N.C.F., K.A.N., E.E.R., A.H., and C.J.J. acknowledge support from the National Science Foundation under grant number CHE-1905172. M.C acknowledges support from the National Science Foundation under grant number CHE-1945271.

References

(1) Seinfeld, J. H. Air pollution: A half century of progress. *AIChE J* **2004**, *50*, 1096–1108.

(2) Rückerl, R.; Schneider, A.; Breitner, S.; Cyrys, J.; Peters, A. Health effects of particulate air pollution: A review of epidemiological evidence. *Inhal. Toxicol.* **2011**, *23*, 555–592.

(3) IPCC: Climate Change 2013: The Physical Science Basis. Contribution of Working Group I to the Fifth Assessment Report of the Intergovernmental Panel on Climate Change. 2013.

(4) Kulmala, M. et al. Direct Observations of Atmospheric Aerosol Nucleation. *Science* **2013**, *339*, 943–946.

(5) Zhang, R.; Suh, I.; Zhao, J.; Zhang, D.; Fortner, E.; Tie, X.; Molina, L.; Molina, M. Atmospheric new particle formation enhanced by organic acids. *Science* **2004**, *304*, 1487–90.

(6) Zhang, R. Getting to the Critical Nucleus of Aerosol Formation. *Science* **2010**, *328*, 1366–1367.

(7) Riipinen, I.; Yli-Juuti, T.; Pierce, J. R.; Petäjä, T.; Worsnop, D. R.; Kulmala, M.; Donahue, N. M. The contribution of organics to atmospheric nanoparticle growth. *Nat. Geosci.* **2012**, *5*, 453–458.

(8) Metzger, A.; Verheggen, B.; Dommen, J.; Duplissy, J.; Prevot, A. S.; Weingartner, E.; Riipinen, I.; Kulmala, M.; Spracklen, D. V.; Carslaw, K. S., et al. Evidence for the role of organics in aerosol particle formation under atmospheric conditions. *Proc. Natl. Acad. Sci. U.S.A* **2010**, *107*, 6646–6651.

(9) Elm, J.; Kurten, T.; Bilde, M.; Mikkelsen, K. V. Molecular interaction of pinic acid

with sulfuric acid: Exploring the thermodynamic landscape of cluster growth. *J. Phys. Chem. A* **2014**, *118*, 7892–7900.

(10) Carlton, A. G.; Bhave, P. V.; Napelenok, S. L.; Edney, E. O.; Sarwar, G.; Pinder, R. W.; Pouliot, G. A.; Houyoux, M. Model representation of secondary organic aerosol in CMAQv4. 7. *Environ. Sci. Technol* **2010**, *44*, 8553–8560.

(11) Pun, B. K.; Wu, S.-Y.; Seigneur, C.; Seinfeld, J. H.; Griffin, R. J.; Pandis, S. N. Uncertainties in modeling secondary organic aerosols: Three-dimensional modeling studies in Nashville/Western Tennessee. *Environ. Sci. Technol* **2003**, *37*, 3647–3661.

(12) Hallquist, M.; Wenger, J. C.; Baltensperger, U.; Rudich, Y.; Simpson, D.; Claeys, M.; Dommen, J.; Donahue, N.; George, C.; Goldstein, A., et al. The formation, properties and impact of secondary organic aerosol: current and emerging issues. *Atmos. Chem. Phys.* **2009**, *9*, 5155–5236.

(13) Ehn, M.; Thornton, J. A.; Kleist, E.; Sipilä, M.; Junninen, H.; Pullinen, I.; Springer, M.; Rubach, F.; Tillmann, R.; Lee, B., et al. A large source of low-volatility secondary organic aerosol. *Nature* **2014**, *506*, 476–479.

(14) McFiggans, G. Involatile particles from rapid oxidation. *Nature* **2014**, *506*, 442–443.

(15) Crounse, J. D.; Nielsen, L. B.; Jørgensen, S.; Kjaergaard, H. G.; Wennberg, P. O. Autoxidation of organic compounds in the atmosphere. *J. Phys. Chem. Lett.* **2013**, *4*, 3513–3520.

(16) Christoffersen, T.; Hjorth, J.; Horie, O.; Jensen, N.; Kotzias, D.; Molander, L.; Neeb, P.; Ruppert, L.; Winterhalter, R.; Virkkula, A., et al. cis-Pinic acid, a possible precursor for organic aerosol formation from ozonolysis of α-pinene. *Atmos. Environ.* **1998**, *32*, 1657–1661.

(17) Jenkin, M. E.; Shallcross, D. E.; Harvey, J. N. Development and application of a possible mechanism for the generation of cis-pinic acid from the ozonolysis of α-and β-pinene. *Atmos. Environ.* **2000**, *34*, 2837–2850.

(18) Hou, G.-L.; Kong, X.-T.; Valiev, M.; Jiang, L.; Wang, X.-B. Probing the early stages of solvation of cis-pinate dianions by water, acetonitrile, and methanol: a photoelectron spectroscopy and theoretical study. *Phys. Chem. Chem. Phys.* **2016**, *18*, 3628–3637.

(19) Hou, G.-L.; Lin, W.; Deng, S. H. M.; Zhang, J.; Zheng, W.-J.; Paesani, F.; Wang, X.-B. Negative ion photoelectron spectroscopy reveals thermodynamic advantage of organic acids in Facilitating Formation of bisulfate ion clusters: Atmospheric implications. *J. Phys. Chem. Lett.* **2013**, *4*, 779–785.

(20) Hou, G.-L.; Valiev, M.; Wang, X.-B. Deprotonated Dicarboxylic Acid Homodimers: Hydrogen Bonds and Atmospheric Implications. *J. Phys. Chem. A* **2016**, *120*, 2342–2349.

(21) Hou, G.-L.; Lin, W.; Wang, X.-B. Direct Observation of Hierarchic Molecular Interactions Critical to Biogenic Aerosol Formation. *Commun. Chem* **2018**, *1*, 37.

(22) Passananti, M.; Zapadinsky, E.; Zanca, T.; Kangasluoma, J.; Myllys, N.; Rissanen, M. P.; Kurtén, T.; Ehn, M.; Attoui, M.; Vehkamäki, H. How well can we predict cluster fragmentation inside a mass spectrometer? *Chem. Commun.* **2019**, *55*, 5946–5949.

(23) Zanca, T.; Kubečka, J.; Zapadinsky, E.; Passananti, M.; Kurtén, T.; Vehkamäki, H. Highly oxygenated organic molecule cluster decomposition in atmospheric pressure interface time-of-flight mass spectrometers. *Atmos. Meas. Tech.* **2020**, *13*, 3581–3593.

(24) Olah, G. A.; Dunne, K.; Mo, Y.; Szilagyi, P. Stable carbocations. CXXVIII. Protonated acyclic carboxylic acid anhydrides and their cleavage to oxocarbenium ions. Question of the formyl cation in superacid media. *J. Am. Chem. Soc.* **1972**, *94*, 4200–4205.

(25) Prakash, G. S.; Rasul, G.; Liang, G.; Olah, G. ^{13}C NMR spectroscopic and Density Functional Theory (DFT), ab initio, and IGLO theoretical study of protonated cycloalkylcarboxylic acids (carboxonium ions) and their acyl cations (oxocarbenium ions). *J. Phys. Chem.* **1996**, *100*, 15805–15809.

(26) Mackay, G. I.; Hopkinson, A. C.; Bohme, D. K. Acid catalysis in the gas phase: dissociative proton transfer to formic and acetic acid. *J. Am. Chem. Soc.* **1978**, *100*, 7460–7464.

(27) Middlemiss, N. E.; Harrison, A. G. The structure and fragmentation of protonated carboxylic acids in the gas phase. *Can. J. Chem.* **1979**, *57*, 2827–2833.

(28) Klumpp, D. A.; Lau, S.; Garza, M.; Schick, B.; Kantardjieff, K. Electrophilic Chemistry of Biologically Important α-Ketoacids. *J. Org. Chem.* **1999**, *64*, 7635–7637.

(29) Pérez, P. Relationship between superelectrophilicity and the electrophilicity index of isolated species. *J. Org. Chem.* **2004**, *69*, 5048–5053.

(30) Sekiguchi, O.; Bakken, V.; Uggerud, E. Decomposition of protonated formic acid: One transition state—Two product channels. *J. Am. Soc. Mass Spectrom.* **2004**, *15*, 982–988.

(31) Hings, S.; Wrobel, W.; Cross, E.; Worsnop, D.; Davidovits, P.; Onasch, T. CCN activation experiments with adipic acid: effect of particle phase and adipic acid coatings on soluble and insoluble particles. *Atmos. Chem. Phys.* **2008**, *8*, 3735–3748.

(32) Waller, S. E.; Yang, Y.; Castracane, E.; Racow, E. E.; Kreinbihl, J. J.; Nickson, K. A.; Johnson, C. J. The Interplay Between Hydrogen Bonding and Coulombic Forces in Determining the Structure of Sulfuric Acid-Amine Clusters. *J. Phys. Chem. Lett.* **2018**, *9*, 1216–1222.

(33) Waller, S. E.; Yang, Y.; Castracane, E.; Kreinbihl, J. J.; Nickson, K. A.; Johnson, C. J. Electrospray Ionization-Based Synthesis and Validation of Amine-Sulfuric Acid Clusters of Relevance to Atmospheric New Particle Formation. *J. Am. Soc. Mass Spectrom.* **2019**, *30*, 2267–2277.

(34) Frisch, M. J. et al. Gaussian 16 Revision A.03. 2016.

(35) Kreinbihl, J. J.; Frederiks, N. C.; Waller, S. E.; Yang, Y.; Johnson, C. J. Establishing the structural motifs present in small ammonium and aminium bisulfate clusters of relevance to atmospheric new particle formation. *J. Chem. Phys.* **2020**, *153*, 034307.

(36) Johnson, C. J.; Johnson, M. A. Vibrational spectra and fragmentation pathways of size-selected, D_2-tagged ammonium/methylammonium bisulfate clusters. *J. Phys. Chem. A* **2013**, *117*, 13265–13274.

(37) DeBlase, A. F.; Bloom, S.; Lectka, T.; Jordan, K. D.; McCoy, A. B.; Johnson, M. A. Origin of the diffuse vibrational signature of a cyclic intramolecular proton bond: Anharmonic analysis of protonated 1,8-disubstituted naphthalene ions. *J. Chem. Phys.* **2013**, *139*, 024301.

(38) Spieler, S.; Duong, C. H.; Kaiser, A.; Duensing, F.; Geistlinger, K.; Fischer, M.; Yang, N.; Kumar, S. S.; Johnson, M. A.; Wester, R. Vibrational predissociation spectroscopy of cold protonated tryptophan with different messenger tags. *J. Phys. Chem. A* **2018**, *122*, 8037–8046.

(39) Thomas, M.; Brehm, M.; Fligg, R.; Vöhringer, P.; Kirchner, B. Computing vibrational spectra from ab initio molecular dynamics. *Phys. Chem. Chem. Phys.* **2013**, *15*, 6608–6622.

(40) Roscioli, J. R.; McCunn, L. R.; Johnson, M. A. Quantum Structure of the Intermolecular Proton Bond. *Science* **2007**, *316*, 249–254.

(41) Kreinbihl, J. J.; Frederiks, N. C.; Johnson, C. J. Hydration motifs of ammonium bisulfate clusters show complex temperature dependence. *J. Chem. Phys.* **2021**, *154*, 014304.

(42) Yang, Y.; Johnson, C. J. Hydration motifs of ammonium bisulfate clusters of relevance to atmospheric new particle formation. *Faraday Discuss.* **2019**, *217*, 47–66.

(43) Chen, L.; Fournier, J. A. Probing Hydrogen-Bonding Interactions within Phenol-Benzimidazole Proton-Coupled Electron Transfer Model Complexes with Cryogenic Ion Vibrational Spectroscopy. *J. Phys. Chem. A* **2021**, *125*, 9288–9297.

(44) Leavitt, C. M.; DeBlase, A. F.; Johnson, C. J.; van Stipdonk, M.; McCoy, A. B.; Johnson, M. A. Hiding in Plain Sight: Unmasking the Diffuse Spectral Signatures of the Protonated N-Terminus in Isolated Dipeptides Cooled in a Cryogenic Ion Trap. *J. Phys. Chem. Lett.* **2013**, *4*, 3450–3457.

(45) Chen, L.; Ma, Z.; Fournier, J. A. Origins of the diffuse shared proton vibrational signatures in proton-coupled electron transfer model dyad complexes. *J. Chem. Phys.* **2022**, *157*, 154308.

(46) Kamrath, M. Z.; Relph, R. A.; Guasco, T. L.; Leavitt, C. M.; Johnson, M. A. Vibrational predissociation spectroscopy of the H_2-tagged mono- and dicarboxylate anions of dodecanedioic acid. *Int. J. Mass Spectrom.* **2011**, *300*, 91–98.

(47) Yacovitch, T. I.; Heine, N.; Brieger, C.; Wende, T.; Hock, C.; Neumark, D. M.; Asmis, K. R. Communication: Vibrational spectroscopy of atmospherically relevant acid cluster anions: Bisulfate versus nitrate core structures. *J. Chem. Phys.* **2012**, *136*, 241102.

(48) Hou, G.-L.; Wang, X.-B.; Valiev, M. Formation of $(HCOO^-)(H_2SO_4)$ Anion Clusters: Violation of Gas-Phase Acidity Predictions. *J. Am. Chem. Soc.* **2017**, *139*, 11321–11324.

(49) Fatila, E. M.; Twum, E. B.; Karty, J. A.; Flood, A. H. Ion Pairing and Co-facial Stacking Drive High-Fidelity Bisulfate Assembly with Cyanostar Macrocyclic Hosts. *Eur. J. Chem.* **2017**, *23*, 10652–10662.

(50) Ogata, Y.; Harada, T.; Sugimoto, T. Formation of ketenes from carboxylic acids in strong acids. Intermediacy of ketenes in the acid-catalyzed α-chlorination of carboxylic acids. *Can. J. Chem.* **1977**, *55*, 1268–1272.

(51) Craig, R. L.; Nandy, L.; Axson, J. L.; Dutcher, C. S.; Ault, A. P. Spectroscopic determination of aerosol pH from acid–base equilibria in inorganic, organic, and mixed systems. *J. Phys. Chem. A* **2017**, *121*, 5690–5699.

(52) Rindelaub, J. D.; Craig, R. L.; Nandy, L.; Bondy, A. L.; Dutcher, C. S.; Shepson, P. B.; Ault, A. P. Direct measurement of pH in individual particles via Raman microspectroscopy and variation in acidity with relative humidity. *J. Phys. Chem. A* **2016**, *120*, 911–917.